

# Rare-earth/transition-metal magnetic interactions in pristine and (Ni,Fe)-doped $\text{YCo}_5$ and $\text{GdCo}_5$

Christopher E. Patrick,<sup>1</sup> Santosh Kumar,<sup>1</sup> Geetha Balakrishnan,<sup>1</sup> Rachel S. Edwards,<sup>1</sup>  
Martin R. Lees,<sup>1</sup> Eduardo Mendive-Tapia,<sup>1</sup> Leon Petit,<sup>2</sup> and Julie B. Staunton<sup>1,\*</sup>

<sup>1</sup>*Department of Physics, University of Warwick,  
Coventry CV4 7AL, United Kingdom*

<sup>2</sup>*Daresbury Laboratory, Daresbury, Warrington WA4 4AD, United Kingdom*

(Dated: October 5, 2018)

## Abstract

We present an investigation into the intrinsic magnetic properties of the compounds  $\text{YCo}_5$  and  $\text{GdCo}_5$ , members of the  $\text{RETM}_5$  class of permanent magnets (RE = rare earth, TM = transition metal). Focusing on Y and Gd provides direct insight into both the TM magnetization and RE-TM interactions without the complication of strong crystal field effects. We synthesize single crystals of  $\text{YCo}_5$  and  $\text{GdCo}_5$  using the optical floating zone technique and measure the magnetization from liquid helium temperatures up to 800 K. These measurements are interpreted through calculations based on a Green's function formulation of density-functional theory, treating the thermal disorder of the local magnetic moments within the coherent potential approximation. The rise in the magnetization of  $\text{GdCo}_5$  with temperature is shown to arise from a faster disordering of the Gd magnetic moments compared to the antiferromagnetically aligned Co sublattice. We use the calculations to analyze the different Curie temperatures of the compounds and also compare the molecular (Weiss) fields at the RE site with previously published neutron scattering experiments. To gain further insight into the RE-TM interactions, we perform substitutional doping on the TM site, studying the compounds  $\text{RECo}_{4.5}\text{Ni}_{0.5}$ ,  $\text{RECo}_4\text{Ni}$  and  $\text{RECo}_{4.5}\text{Fe}_{0.5}$ . Both our calculations and experiments on powdered samples find an increased/decreased magnetization with Fe/Ni-doping respectively. The calculations further reveal a pronounced dependence on the location of the dopant atoms of both the Curie temperatures and the Weiss field at the RE site.

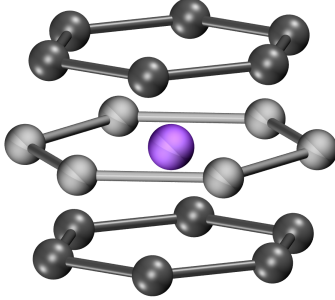


FIG. 1. Ball-and-stick representation of the  $\text{RETM}_5$  crystal structure, showing the RE site (purple) and two TM sublattices:  $\text{TM}_{2c}$  (light gray, in plane with the RE) and  $\text{TM}_{3g}$  (dark gray) where  $2c$  and  $3g$  refer to the Wyckoff positions.

## I. INTRODUCTION

The discovery of the favorable magnetic properties of  $\text{SmCo}_5$  fifty years ago<sup>1</sup> triggered a technological revolution based on rare-earth transition-metal (RE-TM) permanent magnets.<sup>2</sup> In  $\text{SmCo}_5$ , the strong magnetism of Co combines with the large magnetocrystalline anisotropy of localized Sm-4*f* electrons to form an excellent permanent magnet. As well as having provided the blueprint for the development of the now ubiquitous Nd-Fe-B RE-TM magnet class,<sup>3</sup> Sm-Co compounds still play an important role in commercial applications due to their superior high-temperature performance.<sup>4</sup>  $\text{SmCo}_5$  also remains interesting from a fundamental viewpoint, since understanding precisely how the complicated interplay of localized and delocalized electrons affects the anisotropy and magnetization is a significant challenge for electronic structure theory.<sup>5</sup>

$\text{SmCo}_5$  belongs to the  $\text{RETM}_5$  family of permanent magnets which crystallize in the  $\text{CaCu}_5$  structure ( $P6/mmm$ ) whose unit cell is formed of alternating  $\text{RETM}_{2c}/\text{TM}_{3g}$  layers (Fig. 1).<sup>6</sup> This relatively simple crystal structure, paired with the diverse behavior exhibited by magnets with different RE,<sup>7</sup> make the  $\text{RETM}_5$  family an appealing playground for the investigation of RE-TM interactions. In particular, a hierarchy of complexity can be established beginning with RE = Y (i.e. a nonmagnetic RE with no 4*f* electrons), followed by RE = Gd (a half-filled 4*f* shell whose spherical symmetry removes a number of complications involving the spin-orbit interaction and crystal field [CF]), and finally a generic RE with a partly-filled 4*f* shell, like Sm. The different energy scales involved in the interactions<sup>8</sup> allow this hierarchical approach to yield a quite general understanding of the TM-TM, RE-TM

and RE-CF interactions respectively (the label “RE-CF” used in this sense denotes the interactions of the non-spherical  $4f$  charge cloud with the crystal field). An early example of this approach is the empirical subtraction of the magnetization curve of  $\text{YCo}_5$  from other  $\text{RECo}_5$  compounds in order to observe the RE magnetism.<sup>9</sup>

In order to lay the essential groundwork for the future study of compounds where RE-CF interactions are also important, here we concentrate on  $\text{YCo}_5$  and  $\text{GdCo}_5$ . Our strategy is to synthesize and characterize samples and then interpret the results using first-principles calculations based on density-functional theory (DFT). In particular, by applying the disordered local moment (DLM) picture<sup>10</sup> we aim to understand the evolution of magnetic properties with temperature, an aspect which is of obvious practical importance. To this end we have grown single crystals of  $\text{YCo}_5$  and  $\text{GdCo}_5$  using the optical floating zone technique (FZT) and measured the evolution of the magnetization up to 800 K. Our DFT-DLM calculations are able to explain both the contrasting temperature dependences of the two compounds and also the experimentally-observed higher Curie temperature of  $\text{GdCo}_5$ . To further elucidate the RE-TM physics underlying these and other permanent magnets, we have also synthesized polycrystalline samples where Co was substituted with Fe (Ni), which show an increase (decrease) in Curie temperature and magnetization. Our calculations reproduce this behavior, and further explore the dependence of these properties on the crystallographic site occupied by the dopants. Indeed, the calculations find an unusual ferromagnetic RE-TM interaction between Gd and Fe when the atoms occupy nearest neighbor sites.

The rest of this manuscript is organized as follows. In section II we describe the experimental and computational approach used in our study. In section III we report our findings, beginning with pristine  $\text{YCo}_5$  and  $\text{GdCo}_5$  (section III A) and extending to the doped samples (section III G onwards). In section IV we summarize our results and present our conclusions.

## II. EXPERIMENTAL AND THEORETICAL APPROACH

### A. Experimental overview

Owing to its technological importance the  $\text{RECo}_5$  family has been the subject of extensive investigation for several decades, with experiments investigating the temperature dependence of magnetization and anisotropy of pristine  $\text{RECo}_5$  compounds.<sup>9,11–29</sup> However, the growth of

single crystals remains challenging<sup>30,31</sup> and to the best of our knowledge our study represents the first successful attempt to grow single crystals of RECo<sub>5</sub> compounds using the optical FZT. Furthermore, while there are a number of studies investigating specific cases of TM-doped RECo<sub>5</sub> compounds,<sup>32-42</sup> our study tackles both Ni and Fe-doping on both YCo<sub>5</sub> and GdCo<sub>5</sub>. By synthesizing all compounds under the same experimental protocols, we can more rigorously compare trends measured across the series to our calculations.

## B. Experimental approach

Polycrystalline samples of RECo<sub>5-x</sub>Ni<sub>x</sub> (RE = Y, Gd,  $x = 0, 0.5, 1.0$ ) and YCo<sub>4.5</sub>Fe<sub>0.5</sub> were synthesized by arc melting the constituent elements in the appropriate proportions on a water-cooled copper crucible in an argon atmosphere. The ingots were melted, flipped and remelted to ensure homogeneity. No significant changes in weight were observed after melting. Structural characterization was performed by recording powder x-ray diffraction (XRD) patterns of the as-cast samples using a Panalytical Empyrean x-ray diffractometer with a Co target. Single crystals of YCo<sub>5</sub> and GdCo<sub>5</sub> were grown using a four-mirror Xenon arc lamp optical image furnace (CSI FZ-T-12000-X\_VI-VP, Crystal Systems Inc., Japan) using the floating zone technique. The polycrystalline rods for the crystal growth were synthesized by arc melting. The single crystals obtained were aligned using a backscattered X-ray Laue system (Photonic-Science Laue camera). Platelet-shaped crystal samples with the crystallographic  $c$  axis normal to the plane of the plates were obtained from the as-grown crystal boules. The measured lattice constants are reported in Appendix A.

Magnetization measurements were carried out using a Quantum Design Magnetic Property Measurement System (MPMS) superconducting quantum interference device (SQUID) magnetometer. An oven option was used for measurements between 400 and 800 K. Magnetization measurements on the single crystals were performed with the applied magnetic field along the easy axis of magnetization so as to obtain the saturated moment values. Below 400 K the data were collected at intervals of 10 K, while above 400 K the data were recorded while warming at 10 K/minute. In the case of the doped polycrystalline samples, the magnetization versus field curves were recorded using powder samples, with the grains free to rotate under the influence of the magnetic field, so as obtain a best estimate of the saturated magnetic moments.

### C. Theoretical overview

Following on from theoretical studies of  $\text{RECo}_5$  compounds based on experimentally-parameterized CF-models,<sup>9,14,18–22,25,27,36,42–45</sup> first-principles investigations became possible thanks to developments in density-functional theory.<sup>5,46,47</sup> A greater number of first-principles studies of  $\text{YCo}_5$ <sup>48–63</sup> can be found compared to  $\text{GdCo}_5$ ,<sup>5,23,64,65</sup> presumably due to the difficulty of finding an approximate exchange-correlation functional capable of describing the localized Gd-4*f* electrons in DFT. However, most of these studies were performed in a conventional wavefunction-based framework, which is best suited to describing pristine systems at zero temperature. Although dopants can be modeled within this framework via calculations on supercells<sup>51,52,55,56,60</sup> or by using virtual atoms,<sup>50,54</sup> the former approach quickly becomes costly in terms of size convergence while the latter cannot capture the full chemistry of the problem. Meanwhile the calculation of finite-temperature properties in a wavefunction-based framework is generally limited to obtaining critical temperatures based on an assumed Heisenberg model and pairwise interactions.<sup>53,60</sup>

Here, instead of wavefunctions we use the Korringa-Kohn-Rostocker multiple-scattering formulation of DFT<sup>66</sup> combined with the coherent potential approximation (KKR-CPA)<sup>67</sup> and the disordered local moment picture,<sup>10</sup> which reformulates the problem of compositional and thermal magnetic disorder in terms of impurity scattering. Ref. 59 used this approach to study the zero-temperature properties of (Al,Si)-doped  $\text{YCo}_5$ , while Ref. 61 investigated the finite temperature properties of pristine  $\text{YCo}_5$ . The current study combines the computational machinery of the KKR-CPA, the DLM picture, and the local self-interaction correction developed in Ref. 68 to tackle the full problem of the temperature-dependent magnetic properties of pristine and transition-metal-doped  $\text{YCo}_5$  and  $\text{GdCo}_5$ .

### D. Theoretical approach

We follow closely the computational approach described in Ref. 61 and refer the reader to that and other works<sup>10,69–71</sup> for a detailed presentation of the underlying theory. Here we define and describe the key quantities used in our analysis. The technical details of our calculation are reported in Appendix B.

The key concept in the DLM picture is the assignment of a local magnetic moment  $\mu_i$

to each magnetic ion, which we label by the subscript  $i$ . This local moment undergoes fluctuations on the timescale associated with spin-wave excitations, but is stable over the much shorter timescale associated with electron motion.<sup>10</sup> Introducing the unit vectors  $\hat{\mathbf{e}}_i = \boldsymbol{\mu}_i/\mu_i$  to denote the orientations of the local moments, a “good” local moment system is one where the magnitudes  $\{\mu_i\}$  do not depend strongly on the orientations  $\{\hat{\mathbf{e}}_i\}$ .<sup>70</sup> The statistical mechanics of such a system is determined by the thermodynamic potential  $\Omega(\{\hat{\mathbf{e}}_i\})$  which in principle could be obtained from finite-temperature constrained DFT on a large supercell containing many local moments.<sup>10</sup> However, the number of such calculations required to adequately sample the large configurational space spanned by all of the possible orientations  $\{\hat{\mathbf{e}}_i\}$  makes such a direct approach intractable.

To proceed, we instead approximate the statistical mechanics of the local moments with that of an auxiliary system, defined in terms of a model potential

$$\Omega_0(\{\hat{\mathbf{e}}_i\}) = - \sum_i \mathbf{h}_i \cdot \hat{\mathbf{e}}_i. \quad (1)$$

The vectors  $\{\mathbf{h}_i\}$  are parameters of the model with units of energy; they play the role of molecular fields experienced by the local moments, and we refer to them as “Weiss fields”. Although not written explicitly, the Weiss fields depend on temperature. The number of distinct Weiss fields can be chosen to equal the number of crystallographically-distinct sites in the unit cell; however, we emphasize that the sum in equation 1 is over all of the local moments, distributed over the entire crystal.

The potential of equation 1 yields a probability distribution for observing a set of local moment orientations  $\{\hat{\mathbf{e}}_i\}$  as

$$P_0(\{\hat{\mathbf{e}}_i\}) = \prod_i \frac{1}{Z_{0i}} \exp[\boldsymbol{\lambda}_i \cdot \hat{\mathbf{e}}_i] \quad (2)$$

with  $Z_{0i} = (4\pi/\lambda_i) \sinh(\lambda_i)$ , and we have introduced the dimensionless quantities  $\boldsymbol{\lambda}_i = \beta \mathbf{h}_i$  (where  $1/\beta = k_B T$ ). The thermal averages of certain quantities with respect to the model probability distribution  $P_0$  can be performed analytically, e.g. the thermally-averaged orientation of a local moment  $\mathbf{m}_i(T) = \langle \hat{\mathbf{e}}_i \rangle_{0,T}$ :

$$\begin{aligned} \mathbf{m}_i(T) &= \int d\hat{\mathbf{e}}_i \hat{\mathbf{e}}_i \frac{\exp[\boldsymbol{\lambda}_i \cdot \hat{\mathbf{e}}_i]}{Z_{0i}} \prod_{j \neq i} \int d\hat{\mathbf{e}}_j \frac{\exp[\boldsymbol{\lambda}_j \cdot \hat{\mathbf{e}}_j]}{Z_{0j}} \\ &= \hat{\boldsymbol{\lambda}}_i L(\lambda_i) \end{aligned} \quad (3)$$

with  $L(\lambda_i) = \coth(\lambda_i) - 1/\lambda_i$ .  $\mathbf{m}_i(T)$  serve as local order parameters which vanish above the Curie temperature. The integrations are over the angular variables  $(\theta_i, \phi_i)$  where  $\hat{\mathbf{e}}_i = (\sin \theta_i \cos \phi_i, \sin \theta_i \sin \phi_i, \cos \theta_i)$ .

The link between the model parameters  $\{\mathbf{h}_i\}$  and the exact potential  $\Omega(\{\hat{\mathbf{e}}_i\})$  is established through use of the thermodynamic inequality<sup>10</sup>

$$F(T) \leq F_0(T) - \langle \Omega_0 \rangle_{0,T} + \langle \Omega \rangle_{0,T}. \quad (4)$$

Here  $F$  is the exact, unknown free energy. while  $F_0$  is the free energy calculated with the model potential (an analytical function of the Weiss fields). The thermal averages  $\langle \rangle_{0,T}$  of the exact and model potentials are calculated with respect to the model probability distribution, emphasized by the 0 subscript. We define the optimal Weiss fields to be those which minimize the right hand side of equation 4. Performing the minimization yields

$$\mathbf{h}_i = -\nabla_{m_i} \langle \Omega \rangle_{0,T} \quad (5)$$

which can be equivalently written as an integral expression,<sup>10</sup>

$$\mathbf{h}_i = -\frac{3}{4\pi} \int d\hat{\mathbf{e}}_i \langle \Omega \rangle_{0,T}^{\hat{\mathbf{e}}_i} \hat{\mathbf{e}}_i \quad (6)$$

where  $\langle \rangle_{0,T}^{\hat{\mathbf{e}}_i}$  denotes a partial thermal average, i.e. the appropriately-weighted integration over all local moment orientations except  $\hat{\mathbf{e}}_i$ .

Equation 6 is the expression used to evaluate the Weiss fields within the KKR-CPA formalism. One can draw the analogy with the simulation of alloys, where the local moment disorder determined by the probability  $\exp[\boldsymbol{\lambda}_j \cdot \hat{\mathbf{e}}_j]$  is replaced with compositional disorder determined by a probability (concentration)  $c_X$ . The CPA was originally developed with the alloy problem in mind,<sup>66</sup> and its extension to magnetic systems still retains the possibility of including such compositional disorder. Therefore for a given set of  $\{\boldsymbol{\lambda}_i\}$  and concentrations, one can evaluate the Weiss fields subject to the local spin density and coherent potential approximations. More details on the scattering theory underlying the evaluation of equation 6 are given e.g. in Ref. 61.

Since the Weiss fields themselves determine the probability distribution used in the partial thermal average, equation 6 must be solved self-consistently. Indeed the critical (Curie) temperature  $T_C$  for the onset of magnetic order is the highest temperature at which such self-consistent solutions can be found. Once the Weiss fields have been determined at a

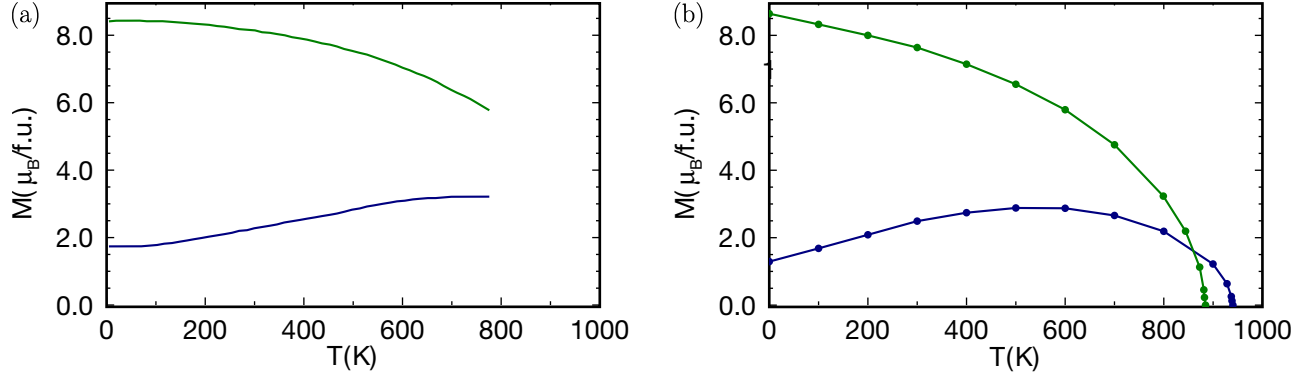


FIG. 2. Magnetization vs temperature (a) measured on single-crystal samples and (b) calculated in the DLM picture, for  $\text{YCo}_5$  (green) and  $\text{GdCo}_5$  (blue). The straight lines connecting points in (b) are guides to the eye.

particular temperature, the model probability distribution  $P_0$  can be fed into additional KKR-CPA calculations to calculate thermal averages of spin and orbital moments (and in principle other quantities such as the torque)<sup>69</sup> as  $\langle A \rangle_{0,T}$ , where  $A$  is the appropriate quantum mechanical operator.

### III. RESULTS AND DISCUSSION

#### A. Magnetization vs. temperature of pristine $\text{YCo}_5$ and $\text{GdCo}_5$

We begin our study with pristine  $\text{YCo}_5$  and  $\text{GdCo}_5$ . The experimentally-determined magnetization vs. temperature ( $MvT$ ) curves are shown in Fig. 2(a). These data were measured for our single crystals in an applied field of 1 or 2 T directed along the easy  $c$ -axis for temperatures below and above 400 K, respectively. As we discuss in Sec. III H, this field is sufficient to saturate the magnetization. We see from Fig. 2(a) that  $\text{YCo}_5$  behaves like an ordinary ferromagnet, with a monotonic decrease in magnetization per formula unit from  $8.41\mu_B$  at 4 K to  $6.38\mu_B$  at 700 K. The magnetization of  $\text{GdCo}_5$  meanwhile increases, from  $1.74\mu_B$  at 4 K to  $3.21\mu_B$  at 700 K.

For the behavior of the magnetization at higher temperatures we refer to previously-reported measurements,<sup>9,12,15</sup> which show the magnetization of  $\text{GdCo}_5$  to start decreasing at temperatures in the region of 700–800 K (a lower value of 600 K was found in Ref. 14). The reported Curie temperatures<sup>9,11,12,14,15</sup> for  $\text{GdCo}_5$  fall in the range 1000–1030 K compared to



	YCo <sub>5</sub>	GdCo <sub>5</sub>
$\mu_{\text{RE}}$	—	-7.32/-0.01
$\mu_{\text{Co}_{2c}}$	1.62/0.15	1.57/0.15
$\mu_{\text{Co}_{3g}}$	1.64/0.06	1.67/0.05
$\mu_{\text{Co}_{3g'}}$	1.63/0.08	1.65/0.07
$\mu_{\text{Tot,calc}}$	8.64	1.29
$\mu_{\text{Tot,exp}}$	8.41 <sup>a</sup>	1.74 <sup>a</sup>
$\mu_{\text{Tot,exp}}$	8.3 <sup>b</sup> 8.3 <sup>c</sup> 8.13 <sup>d</sup> 7.9 <sup>e</sup>	1.55 <sup>c</sup> 1.72 <sup>f</sup> 1.68 <sup>g</sup> 1.42 <sup>h</sup>

<sup>a</sup> Current work, 4 K, optical FZT

<sup>b</sup> Ref. 25, 0 K, r.f. melting + heat treatment + grinding

<sup>c</sup> Ref. 9, 4 K, r.f. melting + heat treatment + grinding

<sup>d</sup> Ref. 24, 0 K, induction zone melting + grinding

<sup>e</sup> Ref. 26, 0 K, plasma jet melting + heat treatment + grinding

<sup>f</sup> Ref. 23, 5 K, r.f. melting + heat treatment + grinding

<sup>g</sup> Ref. 17, 12 K, arc melting + grinding

<sup>h</sup> Ref. 15, 0 K, plasma jet melting + heat treatment + grinding

TABLE I. Magnetic moments in  $\mu_B$  (per atom or formula unit) for pristine YCo<sub>5</sub> and GdCo<sub>5</sub>. The calculations were performed at 0 K for magnetization along the [101] direction. The experimental values have been measured by us or reported previously in the literature; note the 0 K values were obtained by extrapolation. The calculations have been resolved into spin/orbital contributions with the Co atoms labeled as in Fig. 1; note that the magnetization breaks the symmetry of the 3*g* sublattice, giving rise to a distinct contribution (3*g'*) from the Co atom at the  $0\frac{1}{2}\frac{1}{2}$  position.

the lower range of 980–1000 K<sup>9,25,26</sup> reported for YCo<sub>5</sub>. The review article of Ref. 72 gives values of 1014 K and 987 K for the  $T_C$  of GdCo<sub>5</sub> and YCo<sub>5</sub> respectively.

Our calculated  $MvT$  curves for YCo<sub>5</sub> and GdCo<sub>5</sub> are shown in Fig. 2(b). Pleasingly, we see the same contrasting behavior between the compounds as observed experimentally. Our calculated  $T_C$  values are 885 and 940 K for YCo<sub>5</sub> and GdCo<sub>5</sub> respectively, while the 0 K magnetizations are calculated to be  $8.64\mu_B$  and  $1.29\mu_B$ . Table I gives the decomposition of the magnetization into local spin and orbital moment contributions. As shown in Table I and as realized from early experiments,<sup>13</sup> the RE and TM sublattices align antiferromagnetically, accounting for the  $\sim 7\mu_B$  difference between YCo<sub>5</sub> and GdCo<sub>5</sub>.

## B. Comparison of calculations and experiment

Table I also lists magnetizations measured by us and reported in previous literature on single crystals. It is apparent that the calculations find a larger magnetization for  $\text{YCo}_5$  and smaller one for  $\text{GdCo}_5$  than measured experimentally. However, the size of the discrepancy ( $0.4\mu_B$ ) is of the same magnitude as the change in magnetization on applying an empirical orbital polarization correction ( $0.5\text{--}0.8\mu_B/\text{f.u.}$ <sup>48,49,51</sup>), the size of the induced moment on Y ( $\sim 0.3\mu_B$ ,<sup>49,51</sup> which we disregard) and the variation of the magnetization depending on the choice of spherical approximation for the potential ( $\sim 0.2\mu_B$ ).<sup>49</sup> Therefore we find the current level of agreement between calculated and experimental magnetizations to be acceptable. Comparing our experimental magnetizations to previously-reported values we find our values to lie in at the higher end of the range. However, as emphasized by Table I our study is unique using the optical FZT to synthesize the samples.

Regarding  $T_C$ , the calculations reproduce the experimental ordering of  $\text{YCo}_5$  and  $\text{GdCo}_5$  but the calculated values are smaller than the experimentally-reported ones by approximately 100 K. Usually one would expect an overestimate of  $T_C$  in a mean-field approach. A possible reason for this discrepancy is the use of the atomic-sphere approximation (ASA) to describe the potential (App. B). We note that using a more severe muffin tin approximation further reduces the values of  $T_C$  to 774 and 749 K, so conversely a calculation using a more accurate potential might be expected to yield increased values of  $T_C$ . Unfortunately such full-potential calculations are not yet feasible within our computational framework.

An interesting additional consideration is the role of magnetostructural interactions. The data in Fig. 2(b) were calculated using the lattice constants measured at 300 K as reported in Refs. 73 and 74, namely  $a, c = 4.979, 3.972 \text{ \AA}$  for  $\text{GdCo}_5$  and  $a, c = 4.950, 3.986 \text{ \AA}$  for  $\text{YCo}_5$ . For  $\text{GdCo}_5$  we have investigated the effect of lattice thermal expansion, by recalculating the magnetization at temperatures  $> 600 \text{ K}$  using the lattice parameter data given in Ref. 73. The comparison of magnetizations obtained for the fixed or expanding lattices are shown in Fig. 3. When lattice expansion is taken into account, the calculated  $T_C$  increases by 42 K to 982 K. The sensitivity of magnetic coupling to the lattice parameters is explored further in Sec. III D.

As a general note, we see that in the  $T \rightarrow 0$  limit, the gradients of the experimental  $MvT$  curves go to zero whilst those of the calculated curves do not. This behavior is a

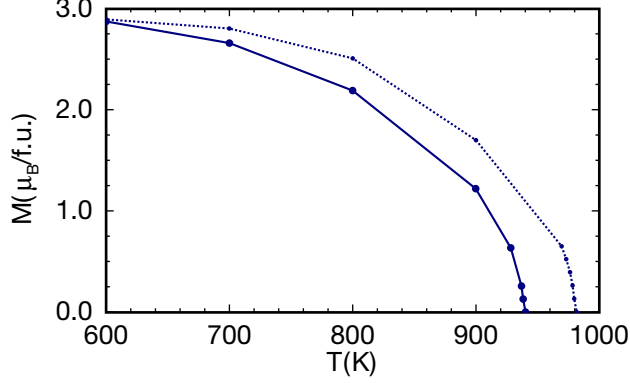


FIG. 3. Magnetization calculated for  $\text{GdCo}_5$  using the 300 K lattice parameters (solid line, larger circles; cf. Fig. 2) or using the temperature-dependent lattice parameters reported in Ref. 73 (dotted line, smaller circles). Note that the temperature-dependent lattice data points  $> 950$  K were all calculated using the same lattice parameters, measured at 1000 K in Ref. 73.

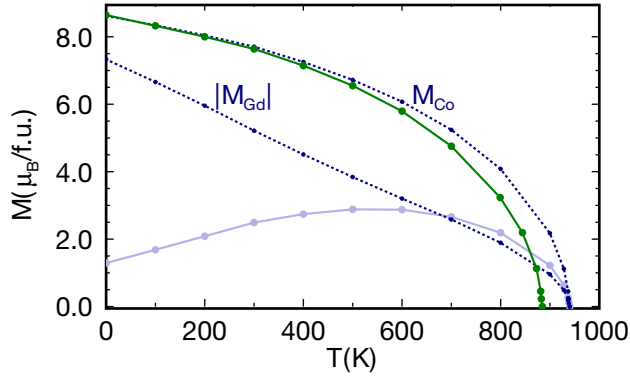


FIG. 4. Decomposition of the magnetization of  $\text{GdCo}_5$  (faint solid blue line) into contributions from the Gd and Co sublattices  $M_{\text{Gd}}$  and  $M_{\text{Co}}$  (dotted lines, small circles). Note that the sublattice magnetizations point antiparallel, so the resultant magnetization is  $M_{\text{Co}} - |M_{\text{Gd}}|$ . The calculated magnetization of  $\text{YCo}_5$  (green solid line) is also shown for comparison.

simple consequence of us using a classical rather than quantized expression to describe the statistical mechanics of the local moments (equation 1).

### C. The disordering of Gd in $\text{GdCo}_5$

In order to better understand the temperature evolution of the magnetism in  $\text{GdCo}_5$  it is instructive to decompose the total magnetization into contributions from the antialigned Gd

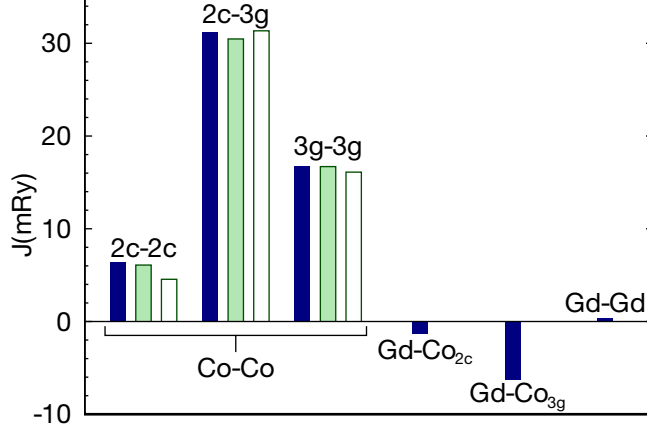


FIG. 5. Calculated values of  $J_{ij}$  in the high-temperature expansion of equation 7 for  $\text{GdCo}_5$  (blue) and  $\text{YCo}_5$  (green). The empty bars are the values of  $J_{ij}$  computed for  $\text{YCo}_5$  using the lattice parameters of  $\text{GdCo}_5$  (see text).

and Co sublattices, as shown in Fig. 4. First we note that below 400 K, the Co contribution  $M_{\text{Co}}$  is indistinguishable from the  $MvT$  curve of  $\text{YCo}_5$ , showing that replacing Y with Gd (i.e. moving from a nonmagnetic to magnetic RE) has a negligible effect on the TM ordering. This observation is in agreement with the established hierarchy of interaction strengths in RE-TM magnets<sup>11</sup> and justifies the practice of subtracting the  $\text{YCo}_5$  curve from  $\text{RECo}_5$  measurements to observe the RE contribution cited in the Introduction.<sup>9</sup> However, as discussed in Sec. III D the RE does have a noticeable effect on the TM sublattice at higher temperatures.

Now considering the Gd contribution, we see the magnitude of the magnetization  $|M_{\text{Gd}}|$  decreases more quickly with temperature than  $M_{\text{Co}}$ . As a result the total magnetization  $M_{\text{Co}} - |M_{\text{Gd}}|$  increases with temperature. As shown in Fig. 4 the decrease in  $|M_{\text{Gd}}|$  is effectively linear up to temperatures of 800 K, while  $M_{\text{Co}}$  displays Brillouin function behavior. Consequently there is a temperature ( $\sim 600$  K) where the gradients of  $M_{\text{Co}}$  and  $|M_{\text{Gd}}|$  are equal, corresponding to a peak in the total magnetization, before  $M_{\text{Co}}$  undergoes a faster decrease close to  $T_{\text{C}}$ . In Sec. III F we reexamine this behavior in terms of the Weiss field at the RE site and compare to low-temperature experimental data.

#### D. Order parameter expansion of $\Omega_0$

The relative strengths of the TM-TM, RE-TM and RE-RE interactions can be quantified by expanding the calculated potential energy  $\langle\Omega\rangle_{0,T}$  in terms of order parameters describing the thermally-averaged local moment at the different sublattices ( $m_i$ ; equation 3). Close to  $T_C$  ( $m_i \rightarrow 0$ ) the expansion can be truncated at second order, i.e.:

$$\begin{aligned} \langle\Omega\rangle_{0,T} \approx & \left( -\frac{1}{2}J_{2c-2c}m_{\text{Co}_{2c}}^2 - J_{2c-3g}m_{\text{Co}_{2c}}m_{\text{Co}_{3g}} \right. \\ & \left. -\frac{1}{2}J_{3g-3g}m_{\text{Co}_{3g}}^2 \right) - \frac{1}{2}J_{\text{Gd-Gd}}m_{\text{Gd}}^2 \\ & - J_{\text{Gd-Co}_{2c}}m_{\text{Gd}}m_{\text{Co}_{2c}} - J_{\text{Gd-Co}_{3g}}m_{\text{Gd}}m_{\text{Co}_{3g}} \end{aligned} \quad (7)$$

where we have decomposed the Co contribution into the two inequivalent  $2c$  and  $3g$  sublattices (Fig. 1), and assumed collinear magnetization of the sublattices. Only the terms in parentheses are required for  $\text{YCo}_5$ . Differentiation of equation 7 with respect to  $m_i$  yields expressions for the Weiss fields through equation 5, conveniently expressed in matrix form:

$$\begin{pmatrix} h_{\text{Co}_{2c}} \\ h_{\text{Co}_{3g}} \\ h_{\text{Gd}} \end{pmatrix} = \begin{pmatrix} \frac{J_{2c-2c}}{2} & \frac{J_{2c-3g}}{2} & \frac{J_{\text{Gd-Co}_{2c}}}{2} \\ \frac{J_{2c-3g}}{3} & \frac{J_{3g-3g}}{3} & \frac{J_{\text{Gd-Co}_{3g}}}{3} \\ J_{\text{Gd-Co}_{2c}} & J_{\text{Gd-Co}_{3g}} & J_{\text{Gd-Gd}} \end{pmatrix} \begin{pmatrix} m_{\text{Co}_{2c}} \\ m_{\text{Co}_{3g}} \\ m_{\text{Gd}} \end{pmatrix}. \quad (8)$$

The denominators of 2 and 3 account for the multiplicities of the  $2c$  and  $3g$  positions. We then obtain the  $J_{ij}$  coefficients from a least-squares fit of the calculated  $\{h_i\}$  values from a training set of  $\{m_i\}$  (equivalently,  $\{\lambda_i\}$ ), and plot them in Fig. 5. It is essential to stress that the  $J_{ij}$  values are not simply describing pairwise interactions, but rather should be thought of as coefficients in the rather general expansion of  $\langle\Omega\rangle_{0,T}$  in equation 7. This point is discussed further in Ref. 75.

Initially focusing on  $\text{GdCo}_5$  (blue bars in Fig. 5), we first note the negative values of  $J_{\text{Gd-Co}_{2c}}$  and  $J_{\text{Gd-Co}_{3g}}$ , as expected for antiferromagnetic alignment. The RE-RE interaction quantified by  $J_{\text{Gd-Gd}}$  is ferromagnetic but negligibly small, i.e. the RE ordering is driven by RE-TM interactions. Interestingly,  $J_{\text{Gd-Co}_{3g}}$  is 4.5 times larger than  $J_{\text{Gd-Co}_{2c}}$ , showing that the dominant RE-TM interaction is not between in-plane nearest neighbors, but rather between the RE and the adjacent pure Co planes. It follows that substituting Co at the  $3g$  positions should have a greater effect on the RE than at the  $2c$  positions, a hypothesis that we test in Sec. III J.

Turning to the TM-TM interaction in GdCo<sub>5</sub>, again we find the largest  $J_{ij}$  to correspond to interplanar interactions, i.e.  $J_{2c-3g}$ . The in-plane interactions  $J_{2c-2c}$ ,  $J_{3g-3g}$  are also ferromagnetic but smaller by  $J_{2c-3g}$  by factors of 5 and 2, respectively. Comparing these  $J_{ij}$  values with those found for YCo<sub>5</sub> (green filled bars in Fig. 5) we find the same ordering of values and similar magnitudes, but the dominant  $J_{2c-3g}$  coefficient of GdCo<sub>5</sub> is larger by 2.4%.

Given that the values of  $J_{ij}$  determine  $T_C$  (discussed in the following section), we investigated the origin of the difference in  $J_{2c-3g}$  by performing a calculation on YCo<sub>5</sub> using the lattice parameters of GdCo<sub>5</sub>. This procedure amounts to increasing the  $a$  parameter by 0.5% and reducing the  $c$  parameter by 0.4%.<sup>73,74</sup> The resulting  $J_{ij}$  values are shown as the empty green bars in Fig. 5. We see that the respective increase and decrease in  $a$  and  $c$  coincide with weakened in-plane interactions ( $J_{2c-2c}$ ,  $J_{3g-3g}$ ). However, the interplanar interaction is strengthened by 2.9%, leading us to attribute the difference in  $J_{2c-3g}$  between GdCo<sub>5</sub> and YCo<sub>5</sub> to be structural in origin. We surmise that the RE can indirectly modify the TM-TM interaction through chemical pressure.

### E. Calculation of $T_C$ from $J_{ij}$

Equation 8 can be used to calculate  $T_C$  by replacing  $m_i = L(\lambda_i) = L(\beta h_i)$  and using the  $m_i \rightarrow 0$  limit,  $L(x) \rightarrow \frac{x}{3}$ . Equation 8 then reduces to an eigenvalue problem, with the smallest  $\beta$  corresponding to  $T_C$ . This approach allows the analysis of the difference in  $T_C$  between GdCo<sub>5</sub> and YCo<sub>5</sub>. For instance, taking the  $J_{ij}$  values obtained for YCo<sub>5</sub> and then replacing  $J_{2c-3g}$  with the larger value obtained for GdCo<sub>5</sub> increases the calculated  $T_C$  from 885 K to 900 K. Further replacing  $J_{2c-2c}$  and  $J_{3g-3g}$  gives a further increase in  $T_C$  to 906 K.

It follows that the remaining 60% of the increase in  $T_C$  observed for GdCo<sub>5</sub> (34 K, to 940 K) must be attributed to the RE-TM and/or RE-RE interaction. We find that the small value of  $J_{\text{Gd-Gd}}$  means that the RE-RE interaction accounts for less than 1 K of the difference, so it is the RE-TM interaction, especially the interplanar interaction characterized by  $J_{\text{Gd-Co}_{3g}}$ , which is responsible. Therefore according to the calculations, although the RE-TM interaction does not affect the Co sublattice magnetization below 400 K (Fig. 4), the interaction is essential to understanding the higher  $T_C$  of GdCo<sub>5</sub>.

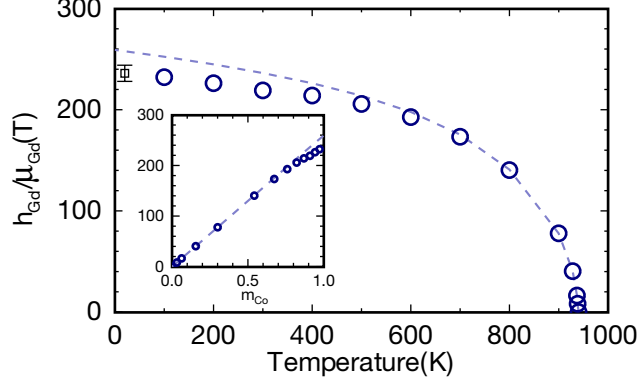


FIG. 6. The molecular field on Gd in GdCo<sub>5</sub>. The open circles show the calculated Weiss fields divided by the local moment magnitudes as a function of temperature. The inset contains the same data as a function of the average Co order parameter. The dashed line shows the expected Weiss field based on the  $J$  expansion of equation 7 and parameters shown in Fig. 5. The open square with error bars in the main panel denotes the molecular field measured by inelastic neutron scattering experiments at 20 K as reported in Ref. 76.

### F. Weiss field on Gd

In Fig. 6 we plot the temperature evolution of  $h_{\text{Gd}}$ , the calculated Weiss field on Gd in GdCo<sub>5</sub>. Since  $h_i$  has units of energy (equation 1) we convert to a field in tesla by dividing by the calculated local moment magnitude  $\mu_{\text{Gd}}$ , which varies from  $7.30$  to  $7.05\mu_B$  from  $T = 0$  K to  $T_C$ . The inset plots the same data against the averaged Co order parameter,  $m_{\text{Co}} = (2m_{\text{Co}_{2c}} + 3m_{\text{Co}_{3c}})/5$ .

The dashed line in Fig. 6 shows the expected behavior of  $h_{\text{Gd}}$  according to equation 8. By construction this fit is accurate close to  $T_C$ , but at temperatures below 600 K deviations are observed, such that  $h_{\text{Gd}}$  is no longer linear in  $m_{\text{Co}}$  (inset). To accurately reproduce the calculated Weiss field at the RE site at these temperatures it is necessary to include higher-order terms<sup>75</sup> in the expansion of equation 7, preventing a straightforward mapping to a Heisenberg-like Hamiltonian.

Although the Weiss fields were introduced as parameters as a means of modeling the local moment statistics, it is reasonable to ask how they compare to the exchange field at the RE site which can be measured via inelastic neutron scattering (INS).<sup>76</sup> Therefore in Fig. 6 we also plot the value of  $236 \pm 8$  T at 20 K which was measured in the INS experiments of

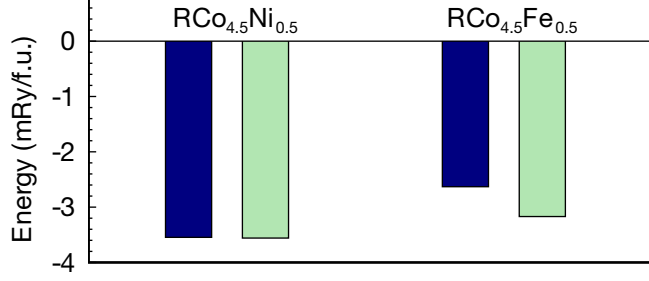


FIG. 7. Calculated energetics of doping of GdCo<sub>5</sub> (blue) or YCo<sub>5</sub> (green) by substituting at a Co<sub>2c</sub> site. The  $y$ -axis zero corresponds to the energy per formula unit when the dopant is substituted at a Co<sub>3g</sub> site, i.e. negative bars imply the dopant is more stable sitting at a Co<sub>2c</sub> site.

Ref. 76. The excellent agreement with the calculated values of  $h_{\text{Gd}}/\mu_{\text{Gd}}$  is perhaps fortuitous and certainly sensitive to the spherical approximation to the potential,<sup>23</sup> but nonetheless gives us confidence in the validity of the local moment description of the RE magnetism.

### G. Substitutional doping of transition metals I: TM sites

We now go beyond the pristine RECo<sub>5</sub> compounds and consider substitutional doping of the transition metals. We have investigated both experimentally and computationally the replacement of Co with its neighboring elements Fe and Ni, considering the compounds RECo<sub>4.5</sub>Ni<sub>0.5</sub>, RECo<sub>4</sub>Ni and RECo<sub>4.5</sub>Fe<sub>0.5</sub>. These low dopant concentrations were chosen to avoid complications arising from structural modification through doping<sup>74</sup> and the low solubility of Fe.<sup>35,39</sup> Even so, due to this low solubility we were unable to synthesize a single-phase sample of GdCo<sub>4.5</sub>Fe<sub>0.5</sub>.

Previous experimental studies<sup>34,37,38</sup> attempted to determine whether the dopants preferentially occupy  $2c$  or  $3g$  sites (Fig. 1) or are distributed equally among the TM sublattices. The neutron diffraction experiments of Ref. 34 on Ni-doped YCo<sub>5</sub> found a preference for Ni substitution at  $2c$  sites (with  $2c/3g$  occupancies of 0.16/0.06 for YCo<sub>4.5</sub>Ni<sub>0.5</sub> and 0.29/0.14 YCo<sub>4</sub>Ni). For Fe-doped YCo<sub>5</sub> we are unaware of similar neutron measurements, but the study of the related compound ThCo<sub>5</sub> in Ref. 37 found a preference for Fe-substitution at  $3g$  sites ( $2c/3g$  occupancies of 0.2/0.5 for YCo<sub>3</sub>Fe<sub>2</sub>). On the other hand Ref. 38 argued that the evolution of lattice parameters of YCo<sub>5</sub> as a function of Fe-doping was consistent with preferential substitution at  $2c$  sites.



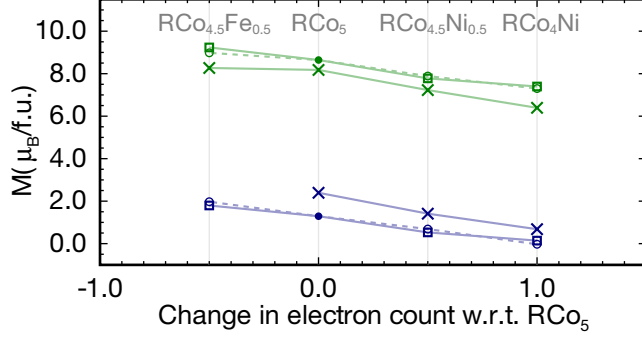


FIG. 8. Low temperature magnetizations of doped  $\text{RECo}_5$  compounds. The crosses show the magnetization of powdered samples in a field of 7 T at 5 K for Fe or Ni-doped  $\text{YCo}_5$  (green) and  $\text{GdCo}_5$  (blue). The circles and squares are the magnetizations calculated where the dopants have been substituted either at  $\text{Co}_{2c}$  or  $\text{Co}_{3g}$  sites respectively.

We have calculated the ground-state (zero temperature) energies of  $\text{RECo}_{4.5}\text{T}_{0.5}$ ,  $\text{T} = \text{Ni}$  or  $\text{Fe}$ , where the dopants were substituted either on the  $2c$  or  $3g$  sites. The energy differences per formula unit between the two cases for  $\text{RE} = \text{Gd}$  and  $\text{Y}$  are shown in Fig. 7. The negative values displayed in Fig. 7 imply that, according to our CPA calculations,  $2c$ -substitution is more stable for both Ni and Fe-doping of both  $\text{GdCo}_5$  and  $\text{YCo}_5$  (blue and green bars). Interestingly, there is a notable difference in the energetics of Fe-doping between  $\text{GdCo}_5$  and  $\text{YCo}_5$ . As discussed in Sec. III J this difference is due to a magnetic energy penalty in placing Fe at  $2c$  sites when Gd is present.

Although the CPA calculations support  $2c$ -ordering, the different conclusions drawn based on experiments<sup>37,38</sup> may indicate a dependence on sample preparation routes. Therefore in order to keep our study general, in the following we present calculations for both  $2c$  and  $3g$  preferential doping. We view these calculations as limiting cases, with the experimentally-realized situation lying somewhere in between.

## H. Substitutional doping of transition metals II: Magnetizations

In Fig. 8 we present the saturation magnetizations measured and calculated for the doped  $\text{RECo}_5$  compounds. As we might expect, the behavior with doping of  $\text{GdCo}_5$  and  $\text{YCo}_5$  is very similar. The general trend is of an increase in magnetization with Fe-doping and a decrease with Ni-doping. This behavior is consistent with a rigid-band picture, noting that

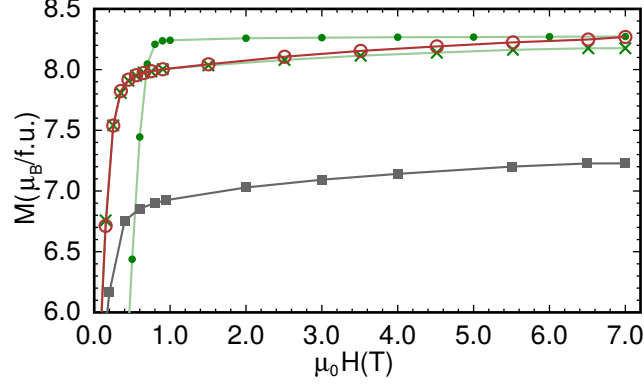


FIG. 9. Magnetization vs. applied field measured at 5 K for single crystal  $\text{YCo}_5$  (green line, filled circles), polycrystalline (powdered)  $\text{YCo}_5$  (green line, crosses),  $\text{YCo}_{4.5}\text{Ni}_{0.5}$  (gray line, squares) and  $\text{YCo}_{4.5}\text{Fe}_{0.5}$  (brown line, empty circles).

in  $\text{YCo}_5$  the  $d$ -band is essentially full in the majority-spin channel and partially occupied in the minority channel;<sup>58</sup> therefore increasing the electron count (through Ni-doping) further populates the minority-spin channel and decreases the overall moment, and vice versa for Fe-doping. The calculated magnetizations for the dopants occupying  $2c$  or  $3g$  sites (circles and squares in Fig. 8) are very similar. The supercell calculations of Ref. 56 found the same behavior, again consistent with the rigid band model.

We now compare the magnetic moments for the polycrystalline (powdered) samples of the pristine compounds ( $\text{YCo}_5$  and  $\text{GdCo}_5$ ) presented in Fig. 8 with the values obtained for the magnetic moments of the single crystals given in Table I. For example, we note that the moment value for the polycrystalline  $\text{YCo}_5$  is  $0.23\mu_B/\text{f.u.}$  lower than the value obtained for the  $\text{YCo}_5$  single crystal. In order to explain this small difference, we focus our attention on the isothermal magnetization plots shown in Fig. 9 obtained at  $T = 5$  K for all the polycrystalline (Fe, Ni)-doped  $\text{YCo}_5$  samples, where for comparison we also plot the magnetization of the  $\text{YCo}_5$  single crystal (green line). During the measurement process, the magnetic field was reduced from 7 to 0 T and the magnetization data were recorded at several field values. It is apparent that none of the  $MvH$  curves for the polycrystalline materials saturate, even at a field of 7 T. In contrast, the  $MvH$  curve for the single crystal saturates above  $\mu_0 H = 1$  T. This demonstrates that it is easier to saturate the magnetization of a single crystal (when  $H$  is applied along the easy axis of magnetization). For a polycrystalline sample of doped or pure  $\text{YCo}_5$  made up of a collection of randomly aligned grains (with

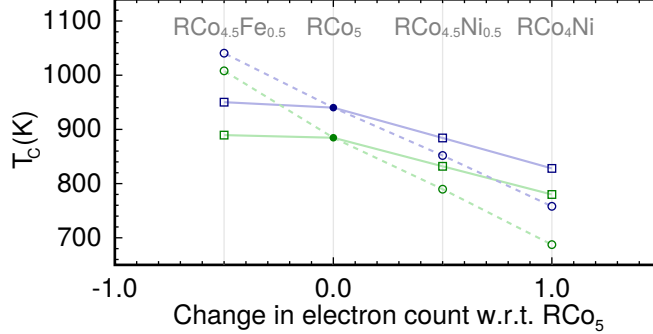


FIG. 10. Curie temperatures calculated for YCo<sub>5</sub> (green) and GdCo<sub>5</sub> (blue) for different doping concentrations, where the dopants have been substituted either at Co<sub>2c</sub> (circles, dashed lines) or Co<sub>3g</sub> (squares, solid lines) sites.

randomly aligned easy axes of magnetization), the magnetization at any field below the anisotropy field will provide a lower bound on the saturation magnetization. For GdCo<sub>5</sub>, the situation is even more complex due to its ferrimagnetic ordering, which can lead to non-collinear Gd and Co spins when the applied field is not parallel to the easy axis.<sup>19</sup> We have also observed that using solid rather than powder polycrystalline samples of YCo<sub>5</sub> leads to even lower values for the magnetic moment at the same  $H$  and  $T$  (data not shown here). Nevertheless, using powder samples one can obtain data that can be used to identify trends, e.g. the variation in the saturation magnetization with doping within a sample series, and the saturation moments obtained lie within a few percent of the single crystal values.

### I. Substitutional doping of transition metals III: $T_C$

In Fig. 10 we present the calculated Curie temperatures for the doped compounds. The variations in  $T_C$  with doping are found to be very similar for RE=Gd and Y, displaying the same  $\sim 60$  K offset as observed for the pristine case and discussed in Sec. III E. However, unlike the magnetization plotted in Fig. 8, the  $T_C$  values show a pronounced dependence on whether the dopants are substituted at the  $2c$  or  $3g$  sites. The largest variations in  $T_C$  occur when the dopants occupy the  $2c$  sites, e.g. increasing by 124 K for YCo<sub>4.5</sub>Fe<sub>0.5</sub> and decreasing by 95 K for YCo<sub>4.5</sub>Ni<sub>0.5</sub>. However, doping with Fe on the  $3g$  sites only raises  $T_C$  by 5 K for YCo<sub>4.5</sub>Fe<sub>0.5</sub>.

Further insight into the behavior of  $T_C$  can be obtained by extending the analysis of

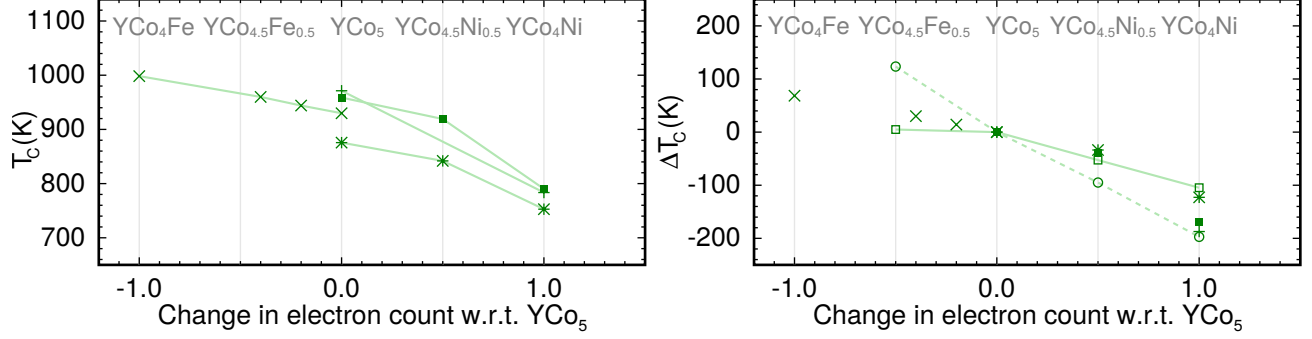


FIG. 11. Curie temperatures of doped  $\text{YCo}_5$ , shown on an absolute scale (left panel) or relative to the  $T_C$  measured/calculated for pristine  $\text{YCo}_5$  (right panel). The experimental  $T_C$  values were previously reported in Refs. 40 (diagonal crosses), 33 (filled squares), 35 (upright crosses) and 32 (asterisks). The right panel additionally shows the calculated  $T_C$  values for doped  $\text{YCo}_5$  (cf. Fig. 10) with the dopants at  $\text{Co}_{2c}$  (circles, dashed lines) or  $\text{Co}_{3g}$  (empty squares, solid lines) sites.

Sec. III D. The appropriate modification of equation 8 is

$$\begin{pmatrix} h_{\text{Co}_{2c}} \\ h_{\text{Co}_{3g}} \\ h_{\text{T}} \\ h_{\text{Gd}} \end{pmatrix} = \begin{pmatrix} \frac{c_{2c}J_{2c-2c}}{2} & \frac{c_{3g}J_{2c-3g}}{2} & \frac{c_{\text{T}}J_{2c-\text{T}}}{2} & \frac{J_{\text{Gd}-\text{Co}_{2c}}}{2} \\ \frac{c_{2c}J_{2c-3g}}{3} & \frac{c_{3g}J_{3g-3g}}{3} & \frac{c_{\text{T}}J_{3g-\text{T}}}{3} & \frac{J_{\text{Gd}-\text{Co}_{3g}}}{3} \\ \frac{c_{2c}J_{2c-\text{T}}}{n} & \frac{c_{3g}J_{3g-\text{T}}}{n} & \frac{c_{\text{T}}J_{\text{T}-\text{T}}}{n} & \frac{J_{\text{Gd}-\text{T}}}{n} \\ c_{2c}J_{\text{Gd}-\text{Co}_{2c}} & c_{3g}J_{\text{Gd}-\text{Co}_{3g}} & c_{\text{T}}J_{\text{Gd}-\text{T}} & J_{\text{Gd}-\text{Gd}} \end{pmatrix} \begin{pmatrix} m_{\text{Co}_{2c}} \\ m_{\text{Co}_{3g}} \\ m_{\text{T}} \\ m_{\text{Gd}} \end{pmatrix} \quad (9)$$

where  $n$  is the multiplicity of the dopant sites (2 or 3 for  $2c$  or  $3g$  doping, respectively). Removing all terms involving Gd gives the expression for  $\text{YCo}_5$ . For the compound  $\text{RECo}_{5-x}\text{T}_x$ , the dopant concentration  $c_{\text{T}}$  is given by  $x/n$ , while the Co concentrations ( $c_{2c}, c_{3g}$ ) equal  $(1 - c_{\text{T}}, 1)$  for  $2c$ -doping and vice versa for  $3g$ -doping.

We proceed as in Sec. III E to obtain the  $J_{ij}$  values and  $T_C$ . Postponing a discussion of  $\text{GdCo}_5$  to the next section, this analysis for  $\text{YCo}_5$  reveals two key points. First, for Ni-doping,  $J_{2c-2c}$ ,  $J_{2c-3g}$  and  $J_{3g-3g}$  only undergo small changes from the pristine case, while the  $J$  parameters coupling to Ni are negligible. Therefore the observed reduction in  $T_C$  with Ni-doping is essentially a dilution effect. We recall from Fig. 5 that the interlayer coupling dominates the magnetic properties. Doping on the  $2c$  site therefore has a larger effect on  $T_C$  simply due to the lower multiplicity of this site; taking  $\text{YCo}_4\text{Ni}$  as an example,  $2c$ -doping reduces the cobalt content in a layer by 50% compared to only 33% with  $3g$ -doping. This difference alone can account for a 20 K reduction in  $T_C$  moving from  $3g$  to  $2c$ -doping.

The second point applies to the Fe-doped compound  $\text{YCo}_{4.5}\text{Fe}_{0.5}$ . When solving the eigenvalue problem of equation 9, the eigenvectors give the relative ordering strengths of the different sublattices. For the cases of  $2c$  and  $3g$ -doping respectively, the normalized  $(h_{\text{Co}_{2c}}, h_{\text{Co}_{3g}}, h_{\text{Fe}})$  eigenvectors are  $(0.49, 0.44, 0.75)$  and  $(0.61, 0.55, 0.58)$ . That is, for  $2c$ -doping the magnetic ordering close to  $T_C$  is dominated by the Fe sublattice, thanks to a large value of  $J_{\text{Fe-Fe}}$  (29 mRy). As we explore in the next section, the presence of Fe at the  $2c$  sites also modifies the exchange field at the RE site.

In Fig. 11 we compare our calculated  $T_C$  for  $\text{YCo}_{5-x}\text{T}_x$  with previously-published experimental data.<sup>32,33,35,40</sup> The experiments also find an increase or decrease in  $T_C$  for Fe or Ni-doping, respectively. As already noted, the calculated  $T_C$  for  $\text{YCo}_5$  is lower than that measured experimentally, and the left panel of Fig. 11 also illustrates the scatter in reported experimental values. Therefore in the right panel of Fig. 11 we plot the same data as a difference relative to the  $T_C$  measured for  $\text{YCo}_5$ , and include our calculated data for  $2c$  or  $3g$ -doping. With the exception of  $\text{YCo}_{4.5}\text{Ni}_{0.5}$  the experimental data points fall in between the  $2c/3g$  limiting cases. We tentatively note that the values of  $T_C$  of Fe-doped  $\text{YCo}_5$  measured in Ref. 40 do not show the large increase predicted for preferential  $2c$  substitution, which would support the conclusion based on  $\text{ThCo}_5$  that  $3g$  substitution is preferable.<sup>37</sup> However, given the uncertainties in measuring and calculating  $T_C$  we acknowledge that such an indirect assignment can only be speculative.

## **J. Substitutional doping of transition metals IV: Modification of the RE-TM interaction through doping**

Aside from modification of the magnetization and  $T_C$ , it is important to establish the effect that substitutional doping has on the RE. For instance, since it is the Sm itself which provides the large anisotropy in  $\text{SmCo}_5$ ,<sup>7</sup> control of the RE is equivalent to controlling the anisotropy. For the current case, it is important to establish whether the difficulty in synthesizing  $\text{GdCo}_{4.5}\text{Fe}_{0.5}$  has a magnetic origin. Therefore we use our calculations to investigate the RE-TM interaction in  $\text{GdCo}_{4.5}\text{T}_{0.5}$  for  $\text{T} = \text{Ni}, \text{Fe}$ . In Fig. 12(a) we show the temperature evolution of the Gd magnetization (cf. Fig. 4 for pristine  $\text{GdCo}_5$ ) for preferential  $2c$  or  $3g$ -doping. In Fig. 12(b) we plot the calculated  $J_{ij}$  parameters of equation 9 which quantify the RE-TM interaction.

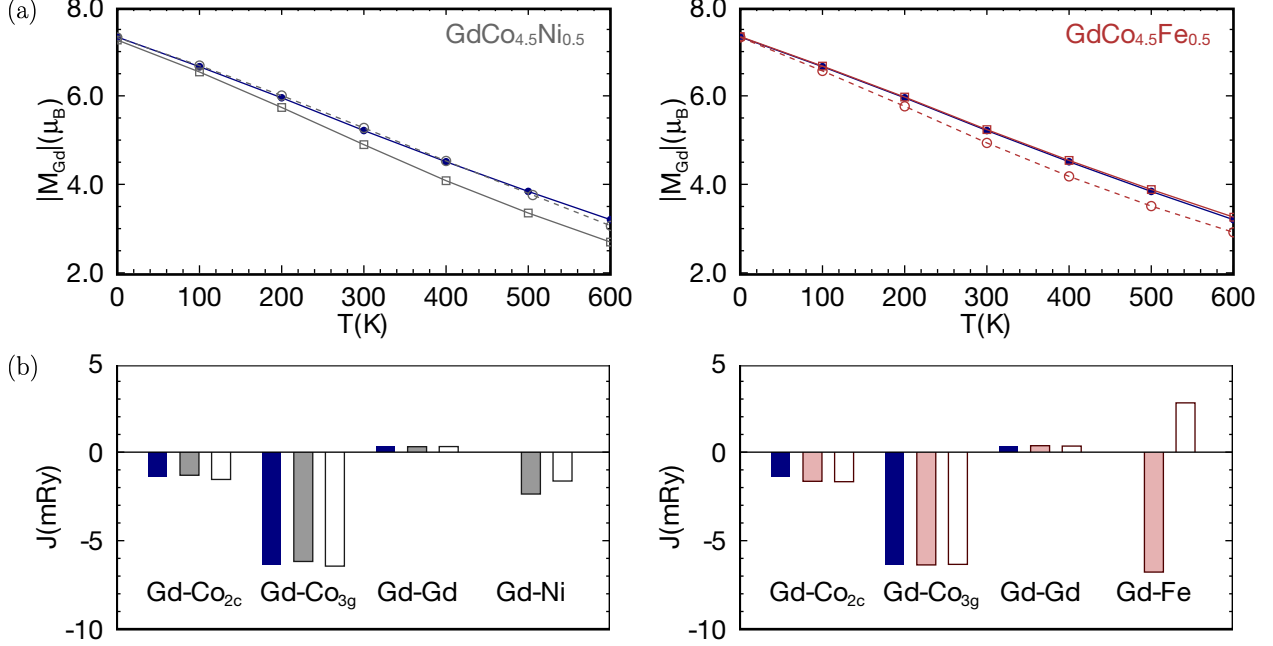


FIG. 12. (a) Absolute magnetization of the Gd sublattice and (b) calculated  $J$  parameters for Ni or Fe-doped  $\text{GdCo}_{4.5}\text{T}_{0.5}$ . Doping on the  $\text{Co}_{2c}$  or  $\text{Co}_{3g}$  site is denoted in (a) by empty circles and squares, respectively, and by empty and light-filled bars in (b). Dark blue filled circles/bars correspond to pristine  $\text{GdCo}_5$ .

Focusing on Ni-doping first (left panels of Fig. 12) we find that doping on the  $2c$  site has a negligible effect on the Gd magnetization. Indeed, we find the value of  $J_{\text{Gd-Ni}}$  to be close to  $J_{\text{Gd-Co}_{2c}}$ , despite the weaker magnetism of Ni. However, doping with Ni on the  $3g$ -site reduces the exchange field at the RE site and causes a faster reduction in the Gd magnetization with temperature. Although the value of  $J_{\text{Gd-Ni}}$  calculated for  $3g$ -doping is larger than that calculated for  $2c$ -doping, it is smaller than  $J_{\text{Gd-Co}_{3g}}$  by almost 50%. Given that it is  $J_{\text{Gd-Co}_{3g}}$  which drives the RE ordering (Sec. III D), this reduction has a noticeable effect on the RE magnetization.

Given that Ni is magnetically weaker than Co, it is not too surprising that we observe a weaker RE-TM interaction. Conversely, given that both  $T_C$  and the zero temperature magnetization increase with Fe-doping, it is tempting to assume that Fe-doping might strengthen the RE-TM interaction, especially when substituted at  $3g$  sites. However, our calculations (right panel of Fig. 12) do not support this view. Doping at the  $3g$  site does give a slightly slower decay of the Gd magnetization due to an enhanced value of  $J_{\text{Gd-Fe}}$ . However, this

value is only 6% larger than  $J_{\text{Gd-Co}_{3g}}$  [filled red bars in Fig. 12(b)], so in  $\text{GdCo}_{4.5}\text{Fe}_{0.5}$  the effect is minimal.

Surprisingly, our calculations further find that Fe-doping at the  $2c$ -site actually weakens the RE-TM interaction and causes a faster temperature decay of the Gd magnetization compared to the pristine case [right panel of Fig. 12(a)]. This unexpected result can be traced to a *positive* value of  $J_{\text{Gd-Fe}}$ , i.e. a ferromagnetic interaction between the RE and the Fe atoms located at the  $2c$  sites. This finding is robust against the choice of spherical approximation to the potential (using the muffin-tin approximation). We note that such a ferromagnetic interaction cannot be accounted for in the standard model of RE-TM interactions based on the hybridization of minority TM- $3d$  with majority RE- $5d$  electrons.<sup>6</sup> The fact that this behavior is only calculated for  $2c$ -doping indicates the existence of a secondary effect when the Fe dopants are placed at nearest neighbor positions to the RE. Such competing magnetic interactions will have a detrimental effect on the solubility of Fe. It is interesting to note that codoping  $\text{GdCo}_5$  with B stabilizes compounds with higher Fe content, given that B occupies precisely these  $2c$  sites.<sup>41</sup>

#### IV. SUMMARY AND CONCLUSIONS

We have studied the  $\text{RECo}_{5-x}\text{T}_x$  family of compounds where RE = Y and Gd and T = Ni and Fe. Our purpose was to probe the TM-TM and RE-TM interactions which govern rare-earth/transition-metal permanent magnets, taking advantage of the relatively simple  $\text{RECo}_5$  crystal structure and lack of crystal-field interactions. We have combined state-of-the-art computational and experimental methods: first-principles calculations based on self-interaction corrected DFT and the disordered local moment picture to calculate magnetic properties for  $0 < T < T_C$ , and single-crystal growth with the optical floating zone technique to obtain high-quality samples.

Beginning with the pristine  $\text{YCo}_5$  and  $\text{GdCo}_5$  compounds, we obtained a theoretical interpretation of the experimentally-measured magnetization vs temperature curves. In particular, the calculations explain the opposite temperature dependences of the two compounds and the ordering of  $T_C$ . The increase in  $\text{GdCo}_5$  magnetization with temperature was shown to arise from a faster decay of the Gd magnetization compared to Co, while the higher  $T_C$  of  $\text{GdCo}_5$  was attributed to both a modification of the lattice parameters due

to the presence of Gd, and also the favorable magnetic coupling between Gd and the Co sublattices. Expanding the potential energy in terms of order parameters showed the dominant magnetic interaction to occur between the planes of the hexagonal  $\text{CaCu}_5$  structure. Comparison of the calculated Weiss fields with the exchange field at the RE site reported from INS measurements<sup>76</sup> found good agreement, supporting the application of the DLM picture to this system.

For the doped systems, both experiments and calculations showed an increase or decrease in magnetization with Fe or Ni-substitution, respectively. The calculations found that this change in magnetization did not depend on whether the dopants were placed at the  $2c$  or  $3g$  crystallographic sites. The calculated values of  $T_C$  also showed the same increase/decrease for Fe/Ni-doping, in agreement with previously-published data for  $\text{YCo}_{5-x}\text{T}_x$ .<sup>32,33,35,40</sup> However, here a dependence on the doping site was observed, with larger changes in  $T_C$  calculated for  $2c$ -doping. For Ni-doping this dependence was explained as a dilution effect, while for Fe-doping the higher  $T_C$  for the  $2c$  case was found to arise from a strong Fe-Fe ferromagnetic interaction.

Examining the RE-TM interaction for the doped  $\text{GdCo}_{5-x}\text{T}_x$  compounds, substituting Ni at the  $3g$  site was found to induce a faster reduction in the Gd magnetization with temperature, as compared to the pristine compound or  $2c$ -doping. However, substituting Fe also showed this faster reduction in magnetization, this time for  $2c$ -doping. The order parameter expansion of the potential energy surface traced the origin of this effect to a ferromagnetic coupling between Gd and Fe at the  $2c$  sites.

Aside from these specific findings described above, the current study has laid the necessary groundwork for the further investigation of the full  $\text{RECo}_5$  family (e.g.  $\text{SmCo}_5$ ), where the RE-CF interactions play a key role. In particular we have established the viability of the experimental and computational protocols needed to synthesize, characterize and model the  $\text{RETM}_5$  permanent magnets. However, our study has also identified a new avenue of study for  $\text{GdCo}_{5-x}\text{Fe}_x$  regarding the Gd-Fe( $2c$ ) interaction. We have raised the possibility that the experimentally-known<sup>41</sup> necessity of codoping  $\text{GdCo}_{5-x}\text{Fe}_x$  with B is related to the calculated competition between ferro and antiferromagnetic RE-TM interactions. For Ni-substitution, although in the current study we have focused on low doping concentrations, by extrapolating the  $\text{GdCo}_5$  data in Fig 8 to higher Ni-doping we can expect a switch from TM to Gd-dominated magnetization at zero temperature, which should yield a compensation



point. There is also a question of whether the TM-magnetization collapses at a critical concentration of Ni or whether it continuously decreases to zero.<sup>54</sup>

As a final note, we point out that the current study has focused on magnetization along a single direction and not addressed anisotropic quantities. Aside from the study of pristine YCo<sub>5</sub> presented in Ref. 61, there is further work to be done regarding the doped compounds. More fundamentally there is the question of the anomalous temperature dependence of the magnetocrystalline anisotropy in GdCo<sub>5</sub>, particularly regarding the role of anisotropic exchange.<sup>21,22,27</sup> Through the combination of our fully-relativistic calculations with high-quality single crystals, we are well-equipped to address such questions in future work.

## ACKNOWLEDGMENTS

The present work forms part of the PRETAMAG project, funded by the UK Engineering and Physical Sciences Research Council, Grant no. EP/M028941/1. Work at Daresbury Laboratory was supported by an EPSRC service level agreement with the Scientific Computing Department of STFC. We acknowledge useful discussions with M. Matsumoto, Prof. G. Rowlands, M. Laver, M. Lueders, Z. Szotek and A. Walton. We thank Dr. A. Vasylenko for his assistance in translating Ref. 33, Dr. M. Ciomaga Hatnean for assistance with single crystal growth and D. A. Duncan and O. J. Parish for preparing initial samples of doped RECo<sub>5</sub> compounds.

## Appendix A: Structural characterization

In Fig. 13 we show the lattice constants  $a$  and  $c$  of the synthesized (polycrystalline) compounds measured by powder x-ray diffraction at room temperature.

## Appendix B: Computational details

Our calculations proceed in two steps. First, a self-consistent, scalar-relativistic calculation is performed on the magnetically-ordered system in order to determine the potentials associated with each atomic species (note that compositionally-disordered systems can be treated at this step with the CPA). Then, these potentials are fed into a non-self-consistent,

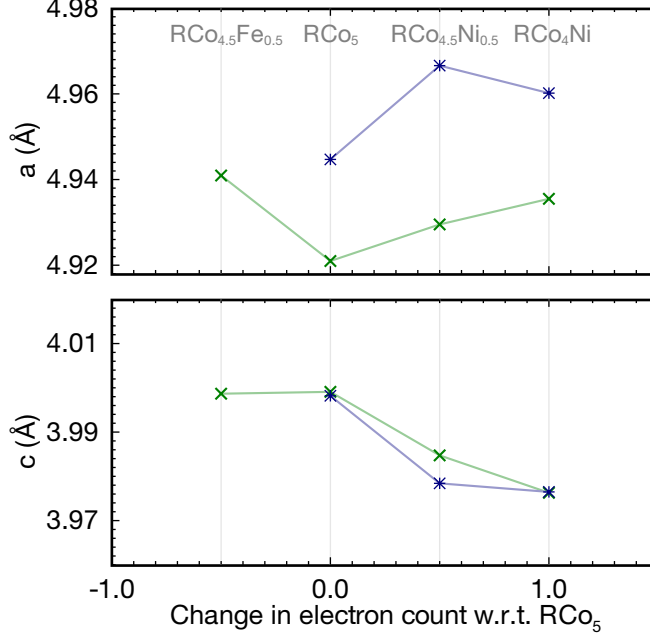


FIG. 13. Lattice parameters (in Å) measured by powder x-ray diffraction for the as-cast samples of transition metal-doped YCo<sub>5</sub> (green, crosses) and GdCo<sub>5</sub> (blue, stars).

fully-relativistic CPA calculation to model the magnetically-disordered system whose local moments are orientated according to the probability distribution specified by  $\{\lambda_i\}$ .

For the first step, we use the local-spin-density approximation for the exchange-correlation potential,<sup>77</sup> treating the 4*f* electrons of Gd with the local-self-interaction correction.<sup>68</sup> The Kohn-Sham potential is determined under a spherical approximation, namely the atomic-sphere approximation (ASA). The ASA sphere radii at the three distinct crystal sites (RE, TM<sub>2c</sub>, TM<sub>3g</sub>) were (1.84, 1.39, 1.42) Å for YTM<sub>5</sub> and (1.85, 1.39, 1.42) Å for GdTM<sub>5</sub>. These values were chosen based on the results of a test calculation performed on YCo<sub>5</sub> with the plane-wave projected-augmented wave code GPAW,<sup>78</sup> observing the radii at which the potentials centered at the three sites showed similar deviations from spherical symmetry subject to the ASA total volume constraint.

We investigated the spherical approximation further by performing calculations under the muffin-tin (MT) approximation for the potential, which prohibits the overlap of different potential spheres and consequently introduces a flat-potential interstitial region. Our calculated critical temperatures based on MT calculations are generally smaller than the ASA ones by  $\sim 100$  K, but trends (e.g. the relative critical temperatures of GdCo<sub>5</sub> and YCo<sub>5</sub>, and the effect of doping on different sites) are preserved. However, the calculated

molecular field at the Gd site is smaller in the MT approximation by almost a factor of 2. Test calculations on the magnetocrystalline anisotropy also find that the MT approximation fails to predict the experimentally-observed easy  $c$ -axis, while the ASA does.<sup>48,49,61</sup>

These scalar-relativistic calculations are performed using the `Hutsepot` KKR-CPA code.<sup>79</sup> The scattering matrices, Green’s function etc. are expanded in a basis of spherical harmonics up to a maximum angular momentum quantum number of  $l = 3$ . Although the KKR-CPA is an all-electron method, there is still a partitioning of electrons into core and valence which determines their treatment within multiple-scattering theory; here the  $4p$  ( $5p$ ) states were treated as valence for Y (Gd). A  $20 \times 20 \times 20$  Brillouin zone sampling was used and a fixed electronic temperature of 400 K in calculating the electronic occupations in the self-consistent calculation.

For the second step in our two-step procedure we solve the fully-relativistic scattering problem<sup>80,81</sup> using the previously-generated “frozen” potentials. Here the  $k$ -space integration is performed to high accuracy using an adaptive sampling algorithm.<sup>82</sup> The electronic states were populated according to the Fermi-Dirac distribution whose temperature was chosen to match the local moment statistics for  $T \geq 400K$  and kept at 300 K otherwise. The integration over angular variables in equation 6 was performed numerically on a  $240 \times 40$  mesh equally spaced in  $\sin \theta_i$  and  $\phi_i$ , and the necessary energy integrations were performed on a rectangular grid extending 2 Rydbergs into the complex plane, using a logarithmic spacing with ten points per decade for the legs of the contour parallel to the imaginary axis. We note that the calculated electronic density could then be used to construct new potentials in an iterative scheme,<sup>83</sup> but here we keep the potentials frozen in line with the local moment picture.

Since the second part of the calculations is fully-relativistic, the thermally-averaged orbital angular momentum  $\langle \mu_{\text{orb}} \rangle_{0,T}$  can develop a nonzero value. However, the frozen potentials do not contain any explicit coupling to orbital angular momentum, e.g. through an empirical orbital polarization correction (OPC) term.<sup>84</sup> It has been observed that including such a term increases the magnitude of the orbital moments in  $\text{YCo}_5$  and also of the anisotropy.<sup>48,49,51</sup> Due to its empirical nature and the fact that it is largely untested for magnetically-disordered systems, we choose not to include an OPC term in the current study.

As mentioned in section IID, the Weiss fields appear on both sides of equation 6, since

the  $\{\lambda_i\}$  values determine  $P_0$ . Following Ref. 61 we obtain the Weiss fields iteratively. For lower temperatures ( $\lambda \gtrsim 2$ ) we find an approach based on fixing  $T$  to be efficient, i.e. the  $\lambda$ -values for the next calculation are obtained from the Weiss fields of the previous (prev) calculation as

$$\lambda_i^{\text{next}} = \beta h_i^{\text{prev}} \quad (\text{B1})$$

for each sublattice  $i$ . For smaller  $\lambda$ -values we find it more efficient to fix  $\lambda$ ; i.e. for sublattice  $i$   $\lambda_i$  is fixed to some value (2, 1, 0.5, 0.1) and  $\lambda_j$  updated until a consistent solution is reached:

$$\lambda_j^{\text{next}} = \lambda_i \frac{h_j^{\text{prev}}}{h_i^{\text{prev}}}. \quad (\text{B2})$$

Finally we note that we have a choice of magnetization direction through the orientations of  $\{\lambda_i\}$ . To make contact with previous work<sup>61</sup> we kept the magnetization direction fixed along [101] and obtain the  $h_i$  magnitudes for the iterative scheme by projecting onto the input  $\lambda_i$  direction. We leave the important questions of magnetocrystalline anisotropy, anisotropic exchange and magnetization anisotropy<sup>21,22,27</sup> for future study.

---

\* j.b.staunton@warwick.ac.uk

- <sup>1</sup> K. Strnat, G. Hoffer, J. Olson, W. Ostertag, and J. J. Becker, *J. Appl. Phys.* **38**, 1001 (1967).
- <sup>2</sup> J. M. D. Coey, *IEEE Trans. Magn.* **47**, 4671 (2011).
- <sup>3</sup> K. H. J. Buschow, in *Handbook of Magnetic Materials*, Vol. 10, edited by K. H. J. Buschow (Elsevier B.V., 1997) Chap. 4, p. 463.
- <sup>4</sup> O. Gutfleisch, M. A. Willard, E. Brück, C. H. Chen, S. G. Sankar, and J. P. Liu, *Adv. Mater.* **23**, 821 (2011).
- <sup>5</sup> M. Richter, *J. Phys. D: Appl. Phys.* **31**, 1017 (1998).
- <sup>6</sup> K. Kumar, *J. Appl. Phys.* **63**, R13 (1988).
- <sup>7</sup> A. Ermolenko, *IEEE Trans. Magn.* **12**, 992 (1976).
- <sup>8</sup> M. D. Kuz'min and A. M. Tishin, in *Handbook of Magnetic Materials*, Vol. 17, edited by K. H. J. Buschow (Elsevier B.V., 2008) Chap. 3, p. 149.
- <sup>9</sup> A. S. Yermolenko, *Fiz. metal. metalloved.* **50**, 741 (1980).
- <sup>10</sup> B. L. Györffy, A. J. Pindor, J. Staunton, G. M. Stocks, and H. Winter, *J. Phys. F: Met. Phys.* **15**, 1337 (1985).

- <sup>11</sup> J. J. M. Franse and R. J. Radwański, in *Handbook of Magnetic Materials*, Vol. 7, edited by K. H. J. Buschow (Elsevier North-Holland, New York, 1993) Chap. 5, p. 307.
- <sup>12</sup> K. Nassau, L. Cherry, and W. Wallace, *J. Phys. Chem. Solids* **16**, 131 (1960).
- <sup>13</sup> E. A. Nesbitt, H. J. Williams, J. H. Wernick, and R. C. Sherwood, *J. Appl. Phys.* **33**, 1674 (1962).
- <sup>14</sup> E. Burzo, *Phys. Rev. B* **6**, 2882 (1972).
- <sup>15</sup> T. Okamoto, H. Fujii, C. Inoue, and E. Tatsumoto, *J. Phys. Soc. Japan* **34**, 835 (1973).
- <sup>16</sup> T. Katayama, M. Ohkoshi, Y. Koizumi, T. Shibata, and T. Tsushima, *Appl. Phys. Lett.* **28**, 635 (1976).
- <sup>17</sup> M. Uehara, *J. Appl. Phys.* **53**, 3730 (1982).
- <sup>18</sup> A. Ermolenko, *IEEE Trans. Magn.* **15**, 1765 (1979).
- <sup>19</sup> R. Radwański, *Physica B+C* **142**, 57 (1986).
- <sup>20</sup> R. Ballou, J. Déportes, B. Gorges, R. Lemaire, and J. Ousset, *J. Magn. Magn. Mater.* **54**, 465 (1986).
- <sup>21</sup> R. Radwański, J. Franse, P. Quang, and F. Kayzel, *J. Magn. Magn. Mater.* **104**, 1321 (1992).
- <sup>22</sup> P. Gerard and R. Ballou, *J. Magn. Magn. Mater.* **104**, 1463 (1992).
- <sup>23</sup> M. D. Kuz'min, Y. Skourski, D. Eckert, M. Richter, K.-H. Müller, K. P. Skokov, and I. S. Tereshina, *Phys. Rev. B* **70**, 172412 (2004).
- <sup>24</sup> W. Frederick and M. Hoch, *IEEE Trans. Magn.* **10**, 733 (1974).
- <sup>25</sup> H. Klein, A. Menth, and R. Perkins, *Physica B+C* **80**, 153 (1975).
- <sup>26</sup> E. Tatsumoto, T. Okamoto, H. Fujii, and C. Inoue, *J. Phys. Colloques* **32**, C1 (1971).
- <sup>27</sup> J. M. Alameda, D. Givord, R. Lemaire, and Q. Lu, *J. Appl. Phys.* **52**, 2079 (1981).
- <sup>28</sup> J. Schweizer and F. Tasset, *J. Phys. F: Met. Phys.* **10**, 2799 (1980).
- <sup>29</sup> M. Yamaguchi, T. Ohta, and T. Katayama, *J. Magn. Magn. Mater.* **31**, 221 (1983).
- <sup>30</sup> J. Miller and A. Austin, *J. Crys. Growth* **18**, 7 (1973).
- <sup>31</sup> T. Katayama and T. Shibata, *J. Crys. Growth* **24**, 396 (1974).
- <sup>32</sup> K. H. J. Buschow and M. Brouha, *J. Appl. Phys.* **47**, 1653 (1976).
- <sup>33</sup> A. S. Yermolenko and A. F. Rojda, *Fiz. metal. metalloved.* **43**, 312 (1977).
- <sup>34</sup> J. Deportes, D. Givord, J. Schweizer, and F. Tasset, *IEEE Trans. Magn.* **12**, 1000 (1976).
- <sup>35</sup> Y. Chuang, C. Wu, and Y. Chang, *J. Less Common Met.* **84**, 201 (1982).
- <sup>36</sup> V. Crisan, V. Popescu, A. Vernes, D. Andreica, I. Burda, and S. Cristea, *J. Alloys Compd.*

- 223**, 147 (1995).
- <sup>37</sup> J. Laforest and J. Shah, *IEEE Trans. Magn.* **9**, 217 (1973).
- <sup>38</sup> F. Rothwarf, H. A. Leupold, J. Greedan, W. E. Wallace, and D. K. Das, *Int. J. Magnetism* **4**, 267 (1973).
- <sup>39</sup> K. N. R. Taylor and C. A. Poldy, *J. Phys. F: Met. Phys.* **5**, 1593 (1975).
- <sup>40</sup> A. Paoluzi, L. Pareti, M. Solzi, and F. Albertini, *J. Magn. Magn. Mater.* **132**, 185 (1994).
- <sup>41</sup> Z. Drzazga, A. Winiarska, and F. Stein, *J. Less Common Met.* **153**, L21 (1989).
- <sup>42</sup> J. P. Liu, X. P. Zhong, F. R. de Boer, and K. H. J. Buschow, *J. Appl. Phys.* **69**, 5536 (1991).
- <sup>43</sup> J. Franse, N. Thuy, and N. Hong, *J. Magn. Magn. Mater.* **72**, 361 (1988).
- <sup>44</sup> Z. Tie-song, J. Han-min, G. Guang-hua, H. Xiu-feng, and C. Hong, *Phys. Rev. B* **43**, 8593 (1991).
- <sup>45</sup> T.-S. Zhao, H.-M. Jin, R. Grössinger, X.-C. Kou, and H. R. Kirchmayr, *J. Appl. Phys.* **70**, 6134 (1991).
- <sup>46</sup> J. Kübler, *Theory of Itinerant Electron Magnetism* (Clarendon Press, Oxford, 2000).
- <sup>47</sup> R. Skomski, P. Manchanda, P. Kumar, B. Balamurugan, A. Kashyap, and D. J. Sellmyer, *IEEE Trans. Magn.* **49**, 3215 (2013).
- <sup>48</sup> L. Nordstrom, M. S. S. Brooks, and B. Johansson, *J. Phys.: Condens. Matter* **4**, 3261 (1992).
- <sup>49</sup> G. H. O. Daalderop, P. J. Kelly, and M. F. H. Schuurmans, *Phys. Rev. B* **53**, 14415 (1996).
- <sup>50</sup> H. Yamada, K. Terao, F. Ishikawa, M. Yamaguchi, H. Mitamura, and T. Goto, *J. Phys.: Condens. Matter* **11**, 483 (1999).
- <sup>51</sup> L. Steinbeck, M. Richter, and H. Eschrig, *Phys. Rev. B* **63**, 184431 (2001).
- <sup>52</sup> K. Uebayashi, K. Terao, and H. Yamada, *J. Alloys Compd.* **346**, 47 (2002).
- <sup>53</sup> A. Kashyap, R. Skomski, R. F. Sabiryanov, S. S. Jaswal, and D. J. Sellmyer, *IEEE Trans. Magn.* **39**, 2908 (2003).
- <sup>54</sup> F. Ishikawa, I. Yamamoto, I. Umehara, M. Yamaguchi, M. Bartashevich, H. Mitamura, T. Goto, and H. Yamada, *Physica B* **328**, 386 (2003).
- <sup>55</sup> P. Larson and I. I. Mazin, *J. Appl. Phys.* **93**, 6888 (2003).
- <sup>56</sup> P. Larson, I. I. Mazin, and D. A. Papaconstantopoulos, *Phys. Rev. B* **69**, 134408 (2004).
- <sup>57</sup> H. Rosner, D. Koudela, U. Schwarz, A. Handstein, M. Hanfland, I. Opahle, K. Koepernik, M. D. Kuz'min, K.-H. Müller, J. A. Mydosh, and M. Richter, *Nature Phys.* **2**, 469 (2006).
- <sup>58</sup> D. Koudela, U. Schwarz, H. Rosner, U. Burkhardt, A. Handstein, M. Hanfland, M. D. Kuz'min,

- I. Opahle, K. Koepernik, K.-H. Müller, and M. Richter, Phys. Rev. B **77**, 024411 (2008).
- <sup>59</sup> D. Benea, O. Isnard, N. Coroian, and V. Pop, J. Magn. Magn. Mater. **322**, 1052 (2010).
- <sup>60</sup> X. B. Liu, Z. Altounian, and M. Yue, J. Appl. Phys. **107**, 09A718 (2010).
- <sup>61</sup> M. Matsumoto, R. Banerjee, and J. B. Staunton, Phys. Rev. B **90**, 054421 (2014).
- <sup>62</sup> P. Kumar, A. Kashyap, B. Balamurugan, J. E. Shield, D. J. Sellmyer, and R. Skomski, J. Phys.: Condensed Matter **26**, 064209 (2014).
- <sup>63</sup> M. Ochi, R. Arita, M. Matsumoto, H. Kino, and T. Miyake, Phys. Rev. B **91**, 165137 (2015).
- <sup>64</sup> T. Beuerle, M. Liebs, K. Hummler, and M. Fähnle, J. Magn. Magn. Mater. **132**, L1 (1994).
- <sup>65</sup> J. Liu, F. de Boer, P. de Châtel, R. Coehoorn, and K. Buschow, J. Magn. Magn. Mater. **132**, 159 (1994).
- <sup>66</sup> B. L. Györfy and G. M. Stocks, in *Electrons in Disordered Metals and at Metallic Surfaces*, edited by P. Phariseau and B. Györfy (Springer US, 1979) Chap. 4, pp. 89–192.
- <sup>67</sup> H. Ebert, D. Ködderitzsch, and J. Minár, Rep. Prog. Phys. **74**, 096501 (2011).
- <sup>68</sup> M. Lüders, A. Ernst, M. Däne, Z. Szotek, A. Svane, D. Ködderitzsch, W. Hergert, B. L. Györfy, and W. M. Temmerman, Phys. Rev. B **71**, 205109 (2005).
- <sup>69</sup> J. B. Staunton, L. Szunyogh, A. Buruzs, B. L. Györfy, S. Ostanin, and L. Udvardi, Phys. Rev. B **74**, 144411 (2006).
- <sup>70</sup> J. B. Staunton, A. Marmodoro, and A. Ernst, J. Phys.: Condens. Matter **26**, 274210 (2014).
- <sup>71</sup> S. N. Khan, J. B. Staunton, and G. M. Stocks, Phys. Rev. B **93**, 054206 (2016).
- <sup>72</sup> K. H. J. Buschow, Rep. Prog. Phys. **40**, 1179 (1977).
- <sup>73</sup> A. Andreev and S. Zadvorkin, Physica B **172**, 517 (1991).
- <sup>74</sup> A. V. Andreev, in *Handbook of Magnetic Materials*, Vol. 8, edited by K. H. J. Buschow (Elsevier North-Holland, New York, 1995) Chap. 2, p. 59.
- <sup>75</sup> E. Mendive-Tapia and J. B. Staunton, Phys. Rev. Lett. **118**, 197202 (2017).
- <sup>76</sup> M. Loewenhaupt, P. Tils, K. Buschow, and R. Eccleston, J. Magn. Magn. Mater. **138**, 52 (1994).
- <sup>77</sup> S. H. Vosko, L. Wilk, and M. Nusair, Can. J. Phys. **58**, 1200 (1980).
- <sup>78</sup> J. Enkovaara *et al.*, J. Phys.: Condens. Matter **22**, 253202 (2010).
- <sup>79</sup> M. Däne, M. Lüders, A. Ernst, D. Ködderitzsch, W. M. Temmerman, Z. Szotek, and W. Hergert, J. Phys.: Condens. Matter **21**, 045604 (2009).
- <sup>80</sup> P. Strange, J. Staunton, and B. L. Györfy, J. Phys. C: Solid State Phys. **17**, 3355 (1984).

- <sup>81</sup> P. Strange, H. Ebert, J. B. Staunton, and B. L. Gyorffy, *J. Phys.: Condens. Matter* **1**, 2959 (1989).
- <sup>82</sup> E. Bruno and B. Ginatempo, *Phys. Rev. B* **55**, 12946 (1997).
- <sup>83</sup> A. Deák, E. Simon, L. Balogh, L. Szunyogh, M. dos Santos Dias, and J. B. Staunton, *Phys. Rev. B* **89**, 224401 (2014).
- <sup>84</sup> O. Eriksson, M. S. S. Brooks, and B. Johansson, *Phys. Rev. B* **41**, 7311 (1990).